

Original Article

Espin distribution as revealed by super-resolution microscopy of stereocilia

Jieyu Qi^{1,2,3}, Liyan Zhang^{1,2}, Fangzhi Tan², Yan Liu², Cenfeng Chu^{2,4}, Weijie Zhu¹, Yunfeng Wang^{5,6}, Zengxin Qi⁷, Renjie Chai^{1,3,8,9,10}

¹Key Laboratory for Developmental Genes and Human Disease, Ministry of Education, Institute of Life Sciences, Southeast University, Nanjing 210096, China; ²iHuman Institute, ShanghaiTech University, Shanghai, China; ³Co-innovation Center of Neuroregeneration, Jiangsu Key Laboratory of Neuroregeneration, Nantong University, Nantong, China; ⁴School of Life Science and Technology, ShanghaiTech University, Shanghai, China; ⁵ENT institute and Otorhinolaryngology Department of Eye & ENT Hospital, Fudan University, Shanghai 200031, China; ⁶NHC Key Laboratory of Hearing Medicine (Fudan University), Shanghai 200031, China; ⁷Department of Neurosurgery, Huashan Hospital, Fudan University, Shanghai 200040, China; ⁸Institute for Stem Cell and Regeneration, Chinese Academy of Science, Beijing, China; ⁹Jiangsu Province High-Tech Key Laboratory for Bio-Medical Research, Southeast University, Nanjing 211189, China; ¹⁰Beijing Key Laboratory of Neural Regeneration and Repair, Capital Medical University, Beijing 100069, China

Received September 5, 2019; Accepted December 9, 2019; Epub January 15, 2020; Published January 30, 2020

Abstract: Auditory hair cells are the mechanical sensors of sound waves in the inner ear, and the stereocilia, which are actin-rich protrusions of different heights on the apical surfaces of hair cells, are responsible for the transduction of sound waves into electrical signals. As a crucial actin-binding and bundling protein, espin is able to cross-link actin filaments and is therefore necessary for stereocilia morphogenesis. Using advanced super-resolution stimulated emission depletion microscopy, we imaged espin expression at the sub-diffraction limit along the whole length of the stereocilia in outer hair cells and inner hair cells in order to better understand espin's function in the development of stereocilia.

Keywords: Espin, stereocilia, super-resolution imaging

Introduction

Located in the organ of Corti, hair cells (HCs) in the basilar membrane are the mechanical sensors for transducing sound vibrations into electrical signals. There are two anatomical and functional types of HCs in the mammalian cochlea-outer hair cells (OHCs) and inner hair cells (IHCs). OHCs are responsible for amplifying the sound entering the cochlea [1, 2], and IHCs are responsible for converting sound vibrations into electrical signals, followed by transmission of sound signals to the auditory brainstem and auditory cortex via auditory nerves [3]. IHCs are arranged in a single row on one side of the modiolus, while three rows of OHCs are arranged on the other side. On both OHCs and IHCs, clusters of hair bundles are present in three rows called stereocilia with increasing heights in a staircase-like manner

[4-7]. Stereocilia are made of parallel actin filaments and associated proteins [7], and the cross-linking of actin filaments is accomplished by actin-bundling proteins like villins, fimbrins/plastins, and espins [7]. Espin is critical in stereociliogenesis and postnatal stereocilia maturation [8, 9], and espin protein expression is restricted to the stereocilia both during morphogenesis and in adulthood [8]. In espin-deficient mice, stereocilia become thin and short [10]. Encoded by a single gene, espin is present in four isoforms (espin 1, 2, 3, 4) that differ in size due to the presence of alternative translation initiation sites [8, 11]. Espin 1, the longest isoform, contains 8 ankyrin repeats in the N-terminus [12], which have been shown to have high binding affinity for myosin 3 at the tips of stereocilia and are associated with the molecular transportation mediated by myosin 3 [13]. Espin 3 is the predominant isoform along

the entire length of the stereocilia in the cochlear hair cells, while espin 2 expression declines prior to birth [11, 13]. The espin 4 isoform primarily mediates the postnatal elongation of stereocilia and the formation of the stereocilia staircase during early postnatal development [14, 15]. However, we know little about the precise distribution of espin in the stereocilia.

Recent advances in super-resolution fluorescence microscopy have allowed the visualization of molecular localization [16]. Stimulated emission depletion (STED) microscopy techniques have been proposed to improve the resolution by selectively inactivating the light scattered by excited fluorophores and thus minimizing the illuminated area at the focal point [17, 18]. STED imaging is capable of detecting signals from a variety of fluorescent dyes at the same time and thus allows for multicolor analyses [19-21]. STED imaging has been used to study the structure and function of cellular proteins [22-25], binding and interactions between proteins [26, 27], the activity and function of organelles [28, 29], and the movement of proteins [20, 28, 30, 31] and other biological macromolecules such as lipids and nucleic acids [32, 33]. Xu and colleagues recently found that actin and its related molecules form periodic structures in the axons of cultured hippocampus neurons using stochastic optical reconstruction microscopy (STORM) [34]. Furthermore, STED has been used to confirm that the periodic cytoskeletal structures in axons and dendrites are present in living neurons [19, 35, 36], and we previously used STED microscopy to show that actin and spectrin form regular ring-like structures in the cuticular plates of HCs [37, 38]. Thus STED microscopy shows great promise for the analysis of the cytoskeleton and its related proteins. In the present study, we used a pan-espin antibody against all isoforms of espin, but which should mainly reflect the signal from espin 3, and STED microscopy in order to visualize the submembrane distribution of espin at the nanoscale level. We observed distinct espin puncta beneath the membrane alongside the actin bundles in the stereocilia. Our findings provide new insights into how espin is organized in stereocilia and suggest that espin might increase the stability of actin filaments in situ.

Materials and methods

Animals

C57BL/6 mice, *Atoh1-Cre* mice, and *Brg1^{flox/flox}* mice of both genders were used. *Brg1^{flox/flox}* mice were mated with *Atoh1-Cre* mice to obtain transgenic *Atoh1-Cre/Brg1^{flox/flox}* mice. Genotyping primers for the transgenic mice were as follows: *Brg1^{flox/flox}*, forward 5'-TCT CAT GCA CAG AGG TCC TG-3', reverse 5'-TAG CCC CTT GAA AGT GAT CC-3'; *Atoh1-WT*, forward 5'-TGA CGC CAC AGC CAC CTG CTA-3', reverse 5'-GGA CAG CTT CTT GTC GTT GTTG-3'; and *Atoh1-Cre*, forward 5'-GCG CAG CGC CTT CAG CAAC-3', reverse 5'-GCC CAA ATG TTG CTG GAT AGT-3'. All experiments were approved by the Institutional Animal Care and Use Committee of Southeast University, China.

Plasmid construction, co-immunoprecipitation and western blotting

Target cDNA sequences were cloned from mouse cochlear cDNA into the vector using Phanta Max Super-Fidelity DNA Polymerase (Vazyme). The C-terminal regions of the target proteins were linked to a 3× FLAG tag, 3× HA tag or fluorescence protein mNeonGreen for further co-immunoprecipitation or immunostaining in human HEK293T cells (American Type Culture Collection). For co-immunoprecipitation, cells were homogenized in lysis buffer containing a mixture of protease inhibitors (Roche). The lysis buffer contained 50 mM Tris, 120 mM NaCl, and 0.5% NP40. Protein supernatant was incubated with Anti-FLAG M2 Magnetic Beads (mouse, Sigma) at 4°C overnight. After immunoprecipitation, protein samples were separated on SDS-PAGE gels (Bio-Rad) and transferred to nitrocellulose filter membranes (0.45 μm, Millipore, Billerica, MA, USA). The membranes were blocked with 5% nonfat dry milk for 2 hours at room temperature and incubated overnight at 4°C with primary antibodies. The membranes were then incubated with HRP-conjugated secondary antibody (1:10,000 dilution; Santa Cruz) for 2 h at room temperature. Signals were visualized using enhanced chemiluminescence (ECL, Pierce, Rockford, IL) and captured on an ImageQuant LAS4000 (GE Healthcare Bioscience). Immunoprecipitation experiments were carried out using rabbit anti-FLAG and rabbit anti-HA antibodies (Proteinte-

ch) and were repeated at least three times to verify the reproducibility of the data.

Immunohistochemistry

Mice were sacrificed with an overdose of pentobarbital sodium (100 mg/kg body weight, i.p.), and the temporal bone was rapidly dissected out. The temporal bone was fixed in 4% paraformaldehyde (in PBS, pH 7.2) for 2 hours and decalcified in 0.5 mM EDTA (pH 8.0) for the 4-8 hours at room temperature. The samples were then cut into pieces and immersed in blocking medium containing 10% donkey serum and 0.5% Triton-X100 in PBS (pH 7.2) for 2 h at room temperature. We used a polyclonal antibody that was raised in rabbits immunized with rat espin 2B and then affinity purified on a column of rat espin 2B covalently attached to CNBr-activated Sepharose 4B [39]. Cochlear tissues were subsequently incubated with espin antibody at 4°C overnight. After complete washing with 0.01 M PBS, the samples were incubated with the corresponding Alexa Fluor 555-conjugated donkey anti-rabbit IgG (H+L) secondary antibody (Thermo Fisher Scientific) for 1 hour at room temperature. Phalloidin conjugated with fluorescent dyes (ATTO 488, ATTO-TEC) was used to label F-actin. Cochlear samples were mounted with Prolong Gold mounting medium (ThermoFisher). Cultured cells were fixed in 4% PFA for 20 minutes at room temperature, and then immunofluorescence was performed with the same procedure as described above.

Scanning electron microscopy

Cochlear specimens from postnatal day (P)14 mice were fixed in fresh 2.5% glutaraldehyde (in PBS, pH 7.2) at 4°C overnight and decalcified in 0.5 mM EDTA (pH 8.0) for 4 hours. The cochlear spiral was cut into pieces and post-fixed in 1% osmic acid (Ted Pella, Inc) for 2 hours at room temperature. Specimens were treated with 2% tannic acid before dehydration in an ethanol gradient (30%, 50%, 70%, 80%, 90%, and 100%) and critical-point drying with liquid CO₂ (CPD300, Leica). After platinum-coating in an electrically conductive material, the cochlear tissues were observed in random fields using a field-emission SEM (Quanta 250, FEI).

Transmission electron microscopy

Cochlear specimens from P30 mice were fixed in 2.5% glutaraldehyde (in PBS, pH 7.2) at 4°C

overnight. After dehydration in an ethanol gradient (30%, 50%, 70%, 80%, 90%, and 100% (v/v)) and acetone (100%), the specimens were embedded in araldite Epon 812 (Ted Pella, Inc). Ultrathin sections were cut using a diamond knife in a direction parallel to the stereocilia and then stained with alcoholic uranyl acetate (Ted Pella, Inc) and alkaline lead citrate (Sigma-Aldrich, Inc). After washing gently with distilled water, random sections were examined with a JEM 1230 transmission electron microscope (JEOL Ltd., Tokyo, Japan).

Image processing and analysis

Immunofluorescence images were exported from LAS X (Leica Microsystems) and further processed using Fiji software (National Institutes of Health). The brightness and contrast of the entire image were linearly adjusted. For quantitatively analyzing the distribution patterns of espin and actin, lines across the structures were drawn and the intensity profiles were measured by FIJI. Intensity profiles were then plotted using GraphPad Prism (GraphPad Software, Inc.).

Results

Espin puncta in the submembrane

Confocal microscopy indicated that espin was expressed in the stereocilia of OHCs and IHCs (**Figure 1A**), which is consistent with previous immunostaining results showing strong co-labeling of espin and F-actin in HCs [40], and this supported the feasibility of using a pan-espin antibody. Under a 100× objective with 9× physical magnification, espin presented with a submembrane distribution along the whole stereocilia, and this was especially obvious in the stereocilia of IHCs, and it showed randomly weak or strong intensities along the stereocilia (**Figure 1B**). Using STED imaging, we also observed that espin was expressed as distinct puncta along the whole length of the stereocilia in OHCs and IHCs, which is a previously unseen distribution pattern (**Figure 1B** and **1C**). Notably, espin was enriched near the membrane, while espin signals were barely detected inside the stereocilia (**Figure 1C**). The submembrane distribution of espin indicates that it might participate in stabilizing the actin network just beneath the plasma membrane in stereocilia. In addition, we found that espin was restricted to the stereocilia, and there was very little sig-

Espin distribution in stereocilia

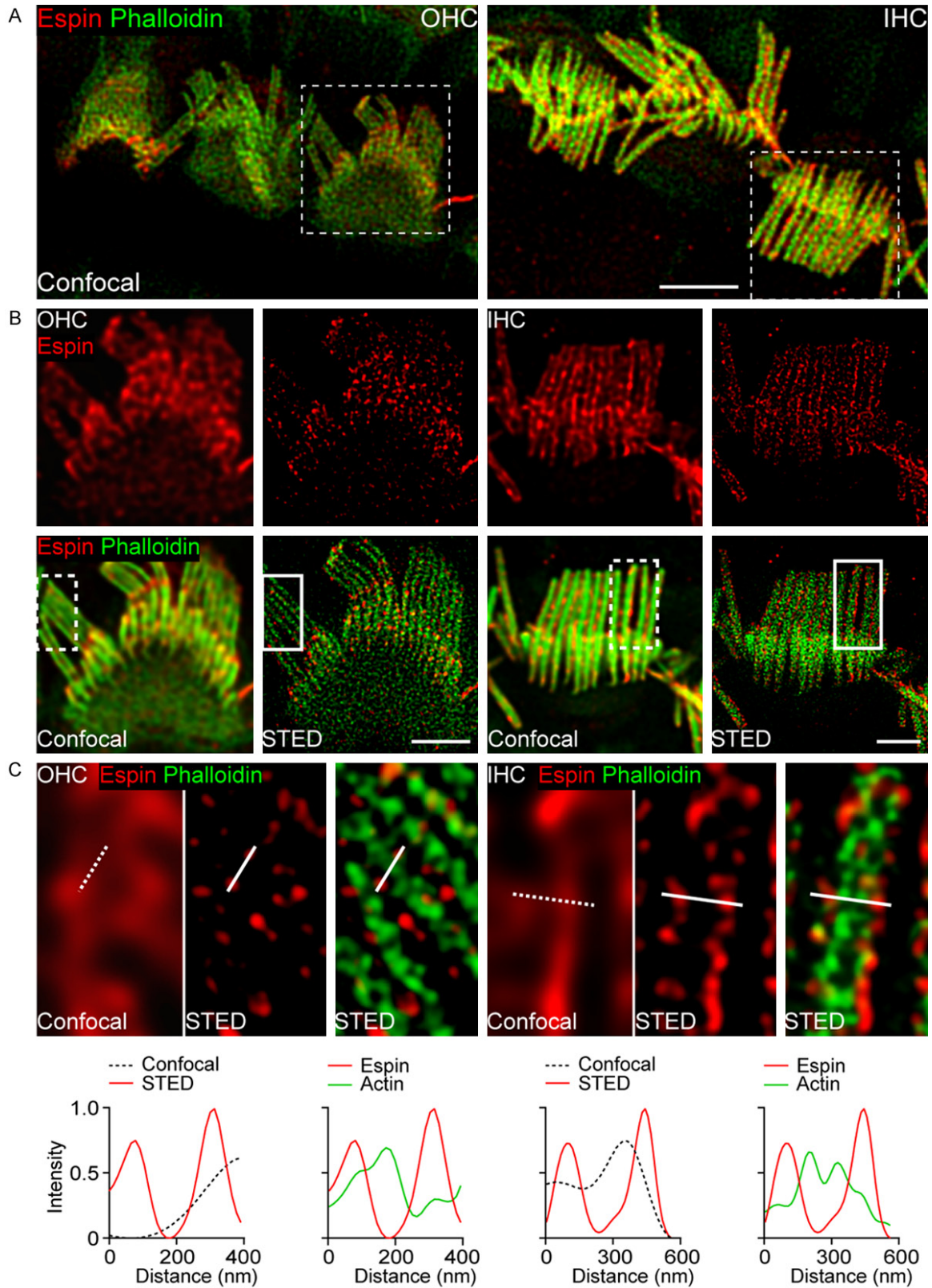


Figure 1. Distribution of espin in the stereocilia of HCs. A. Representative confocal images of espin (red) and F-actin (green) in the OHCs and IHCs from P14 mice. Scale bar, 4 μ m. B. Confocal and STED images of espin (red) and F-actin (green) in OHCs and IHCs from the boxed region indicated in (A). Scale bars, 2 μ m. C. Magnifications of the boxed regions indicated in (B) and intensity profiles from the corresponding lines are shown beneath.

nal in the cuticular plate (**Figure 1B**), suggesting a correlation between espin expression and the structure and function of the stereocilia. We found no significant difference in the distribution pattern of espin in the apical, middle, or basal turns of the cochlea (**Figure 2**). Given the highly conserved organization of espin in different regions of the cochlea, our results suggest that espin outlines the edges of the stereocilia of HCs and might play a role in linking actin to the cell membranes.

It has been reported that espin is required for the assembly and stabilization of parallel actin bundles in the stereocilia [41], and we confirmed this in the present work. In espin-transfected cells, espin tagged with HA or mNeon-Green displayed various fibrous structures (**Figure 3A** and **3B**). Co-immunoprecipitation experiments revealed the interaction between espin and β -actin (**Figure 3C**). The co-labeled espin and actin in HCs showed that espin formed distinct puncta along the bundled actin filaments (**Figure 1**), and in espin-transfected cells, we also found the espin signal along the edge of fibrous actin filaments structures (**Figure 3D**). Transmission electron microscopy imaging of the stereocilia showed the actin-to-membrane links in the region between the actin filament and the plasma membrane, connecting the stereocilium actin core to the cytoplasmic membrane (**Figure 3E**). Similarly, in STED images co-labeled with espin and phalloidin, we found that espin puncta formed tight connections with actin molecules beneath the plasma membrane (**Figure 3F**), and this pattern was observed in the stereocilia at different ages after birth (**Figure 3G**). We thus conclude that espin molecules can interact with actin and maintain the actin cytoskeleton as well as the stereocilia (**Figure 3H**), and we speculate that espin might be involved in actin-membrane linkage.

Espin distribution in mice with disrupted stereocilia

STED imaging showed the espin structure beneath the membrane in both immature and mature mice. To determine if espin plays a functional role, we imaged the espin distribution in transgenic *Atoh1-Brg1*^{-/-} mice, which exhibit stereocilia collapse and suffer from profound deafness [42]. The distribution of espin

in the stereocilia of OHCs from *Atoh1-Brg1*^{-/-} mice (**Figure 4**) showed that espin had scattered expression in the stereocilia similar to wild-type mice, but in these mice the signal could also be detected in the cuticular plate (**Figure 4B**). While the structural distribution of espin in IHCs in *Atoh1-Brg1*^{-/-} mice was comparable to that in control mice, with the morphological structure of IHCs did not show any visible changes in the *Atoh1-Brg1*^{-/-} mice (**Figure 4B**), even though degenerated IHC was occasionally observed in *Atoh1-Brg1*^{-/-} mice (**Figure 5B**). SEM and immunostaining data together showed that OHCs exhibited morphological changes to varying degrees in *Atoh1-Brg1*^{-/-} mice (**Figure 5A** and **5B**). We defined six different types of OHC injury in *Atoh1-Brg1*^{-/-} mice according to the degree of damage to the stereocilia (**Figure 5B** and **5C**). In OHCs with very little damage to the stereocilia (type I), espin remained scattered and was not present in the cuticular plate (**Figure 5C**, Type I). However, espin signals were not only detected in the stereocilia, but also accumulated in the cuticular plate in the OHCs with more severe stereocilia disruption or degeneration (**Figure 5C**, Type II-VI). Our findings suggest that espin is involved in actin organization in stereocilia and support the hypothesis that espin is associated with actin maintenance and normal stereocilia morphology.

Discussion

HCs are characterized by stair-cased stereocilia on the apical surface of the cell body. Sound signals are detected and transduced by these stereocilia, which are the main organizers for mechanotransduction. Stereocilia are mainly composed of actin filaments and are regulated by many actin-binding and bundling proteins like espin [13, 43]. Submembrane proteins play crucial roles in actin stabilization in stereocilia, and longitudinal sections of stereocilia imaged by transmission electron microscopy revealed the proteins between the bundled actin filament and the cytoplasmic membrane. We found that espin was enriched in the submembrane of stereocilia, and was rarely inside the actin bundles, and a similar phenomenon was observed in cultured espin-transfected cells. It appears that espin might participate in the actin-membrane linkage. In addition, radixin, a protein that appears to play a crucial role in

Espin distribution in stereocilia

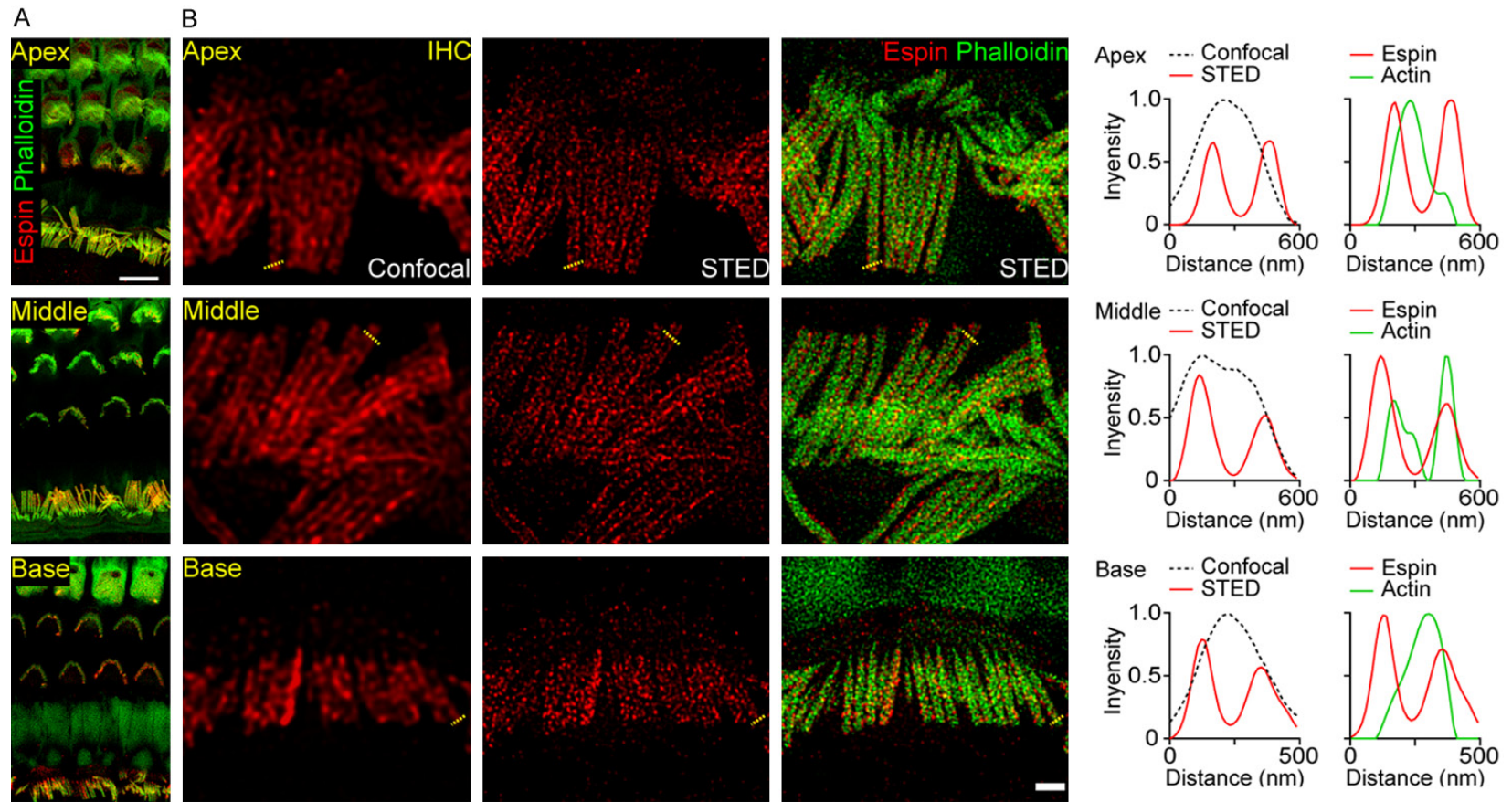
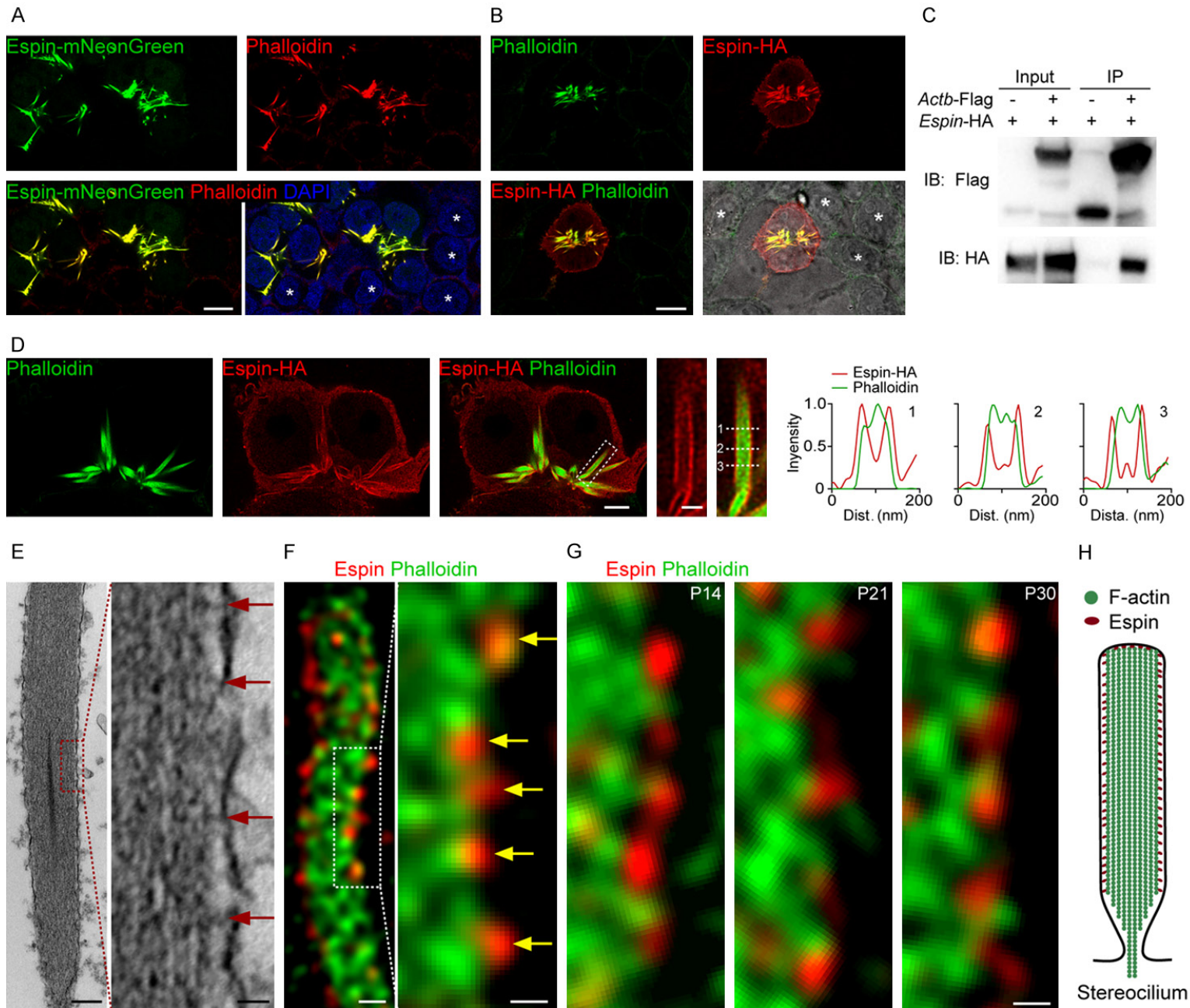


Figure 2. Distribution of espin in different regions of the cochlea. A. Representative confocal images of espin (red) and F-actin (green) in the apical, middle, and basal turns of the cochlea from P14 mice. Scale bar, 5 μm . B. Confocal and STED images of espin (red) and F-actin (green) in IHCs from the apical, middle, and basal turns of the cochlea. Intensity profiles from the corresponding dashed lines are shown right. Scale bar, 1 μm .

Espin distribution in stereocilia



Espin distribution in stereocilia

Figure 3. Actin filaments bundled by espin in stereocilia. A. Representative confocal images of espin-mNeonGreen (green), F-actin (red) and DAPI (blue) in the Espin-mNeonGreen transfected cells. White stars indicated the non-transfected cells surrounding the transfected cells. Scale bar, 10 μ m. B. Representative confocal images of espin-HA (red) and F-actin (green) in the espin-HA transfected cell. The bright-field image to the lower-right shows the individual cells in the captured region. White stars indicate the non-transfected cells surrounding the transfected cell. Scale bar, 10 μ m. C. Co-immunoprecipitation of espin and actin. Human HEK293T cells were transfected with the FLAG, Actb-FLAG, or Espin-HA constructs. Immunoprecipitations were carried out with FLAG antibodies followed by western blotting to detect co-expressed proteins using the HA antibody. Representative images from three independent experiments are shown. D. Representative confocal images of espin-HA (red) and F-actin (green) in the espin-HA-transfected cells, with magnification of the white boxed regions to the right. Scale bars are 4 μ m and 1 μ m, respectively. The dashed lines are numerically labeled, and the corresponding intensity curves along the dashed lines are shown. E. Transmission electron microscopy image of a stereocilium with its magnification. Red arrows indicate the actin-membrane linkages. Scale bars are 200 nm and 25 nm, respectively. F. Representative STED images of a stereocilium with its magnification, co-labeled with espin (red) and F-actin (green). Yellow arrows indicate the espin punctas between the edge of the actin filaments and the membrane. Scale bars are 200 nm and 100 nm, respectively. G. Representative magnified STED images of stereocilia at different development stages after birth, co-labeled with espin (red) and F-actin (green). Scale bar, 100 nm. H. Functional model of espin in the a stereocilium.

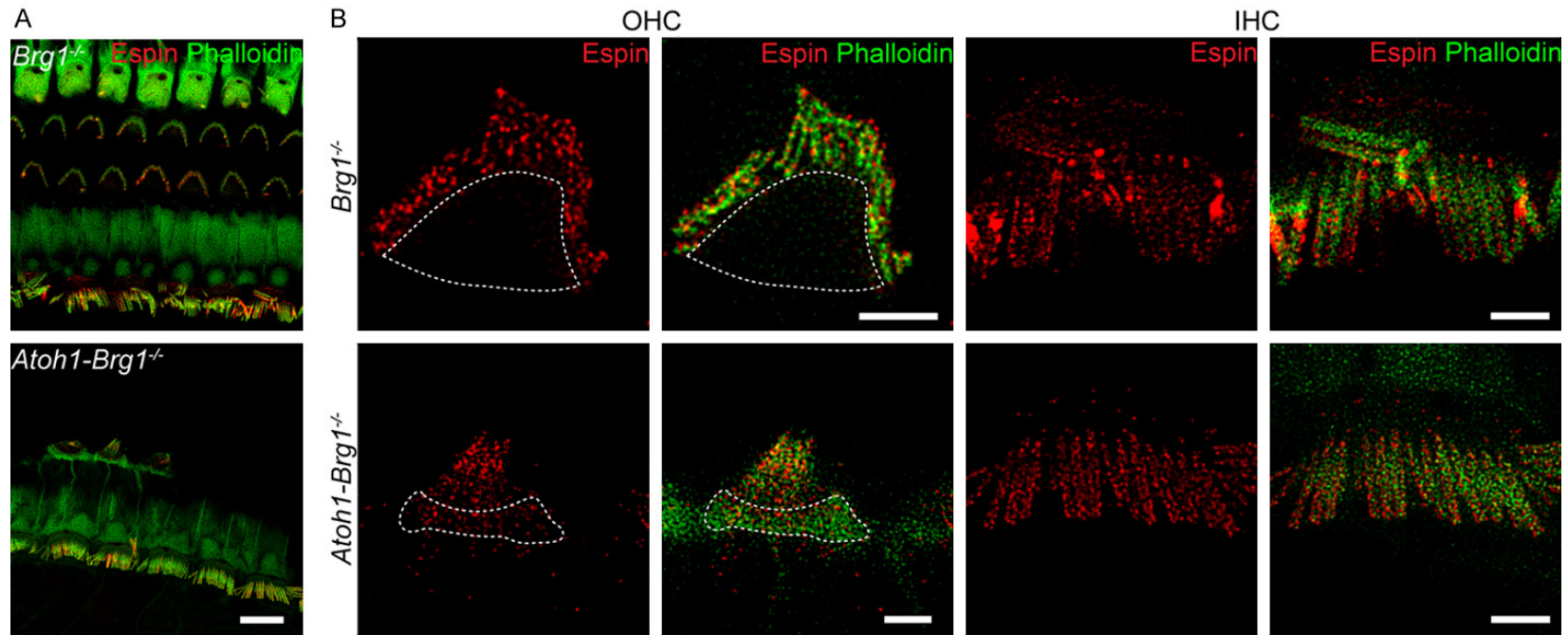


Figure 4. Distribution of espin in deaf mice. A. Representative confocal images of espin (red) and F-actin (green) in the organ of Corti from adult *Brg1^{-/-}* and *Atoh1-Brg1^{-/-}* mice. Scale bar, 10 μ m. B. STED images of espin (red) and F-actin (green) in OHCs and IHCs from adult *Brg1^{-/-}* and *Atoh1-Brg1^{-/-}* mice. Regions indicated by white closed curves show the cuticular plates. Scale bars, 2 μ m.

Espin distribution in stereocilia

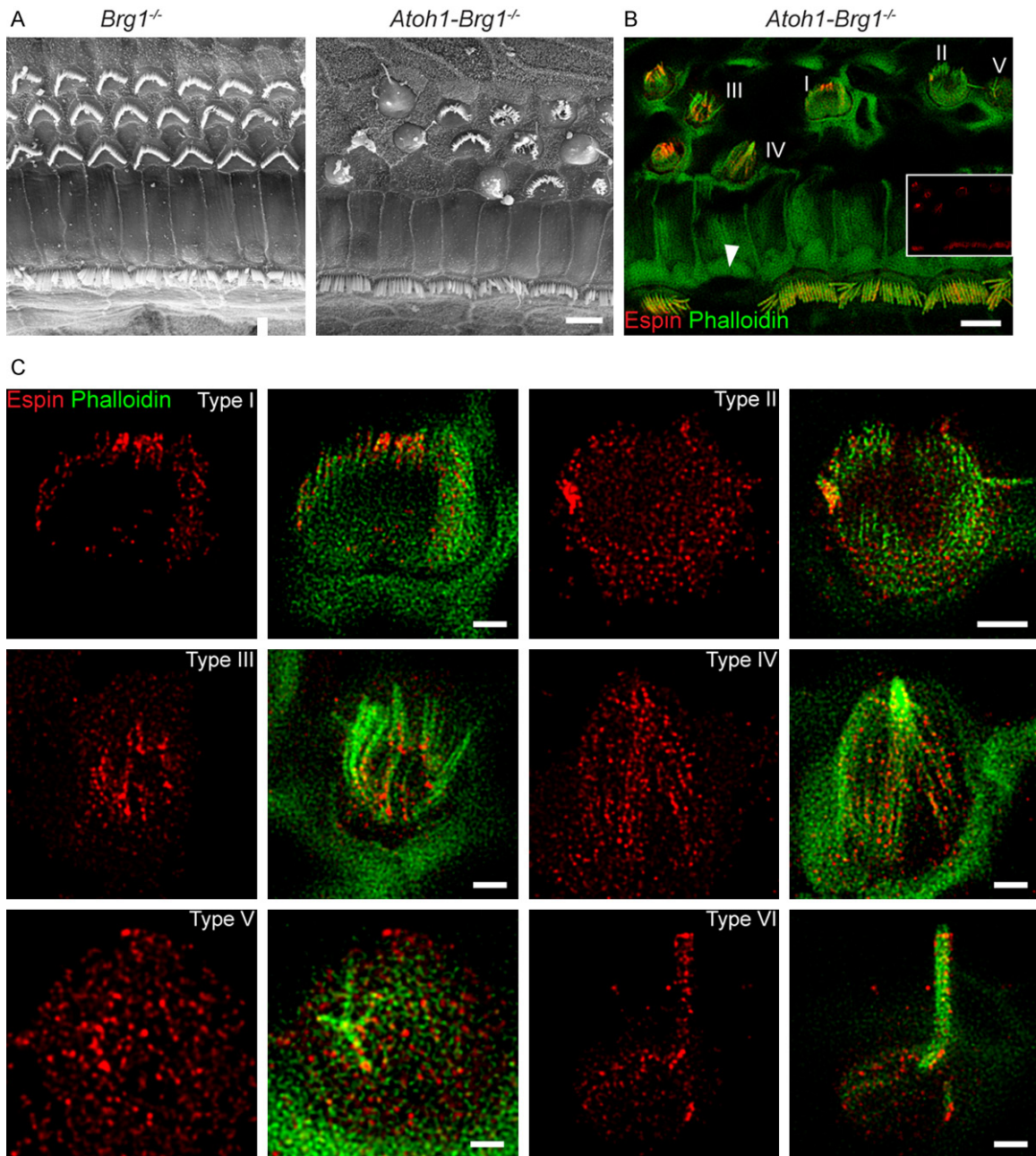


Figure 5. Altered espin distribution in OHCs from *Atoh1-Brg1*^{-/-} mice. A. Representative SEM images of the organ of Corti from adult *Brg1*^{-/-} and *Atoh1-Brg1*^{-/-} mice. Scale bar, 5 μ m. B. Representative confocal images of the organ of Corti from adult *Atoh1-Brg1*^{-/-} mice. The espin signal from the same optical field is shown in the insert image. Red, espin. Green, F-actin. Numbers I-V indicate impaired OHCs with different morphologies. White triangle indicates the occasional missing IHC in adult *Atoh1-Brg1*^{-/-} mice. Scale bar, 5 μ m. C. STED images of espin (red) and F-actin (green) in different OHC morphologies in adult *Atoh1-Brg1*^{-/-} mice. Scale bars, 1 μ m.

anchoring the actin filaments to the plasma membrane [44], has a very similar distribution to espin in stereocilia as imaged by STED microscopy (data not shown). We are currently performing work to determine if there is a relationship between radixin and espin.

Noticeably, espin signals were detected at the tips of the stereocilia, and espin is considered to be involved in the elongation of actin in stereocilia [13, 43] and to be required for targeting myosin 3b to stereocilia tips and for regulating the stereocilia diameter and staircase forma-

tion [45]. Therefore, espin appears to play complicated and crucial roles in actin dynamics and stabilization. In the absence of espin, the length and width of the stereocilia are severely affected [45]. At the same time, we observed a positive correlation between the degree of disordered espin distribution and stereocilia impairment in mice with genetic-related hearing loss. When the actin bundle in the cilia is destroyed, espin spreads from the stereocilia to the apical region of the cytoplasm, suggesting that espin is involved in the assembly and stabilization of the parallel stereociliary actin bundles and thus is required for the formation and maintenance of stereocilia.

Conclusion

In summary, this study characterized the nanoscale espin distribution in the stereocilia using super-resolution STED imaging. Our results show that discontinuous espin clusters in the submembrane of stereocilia are closely related with actin bundling activity. Such spatial organization of espin within stereocilia might play a critical role in stereocilia function and therefore in normal hearing.

Acknowledgements

We thank the Bioimaging Core Facilities of the iHuman Institute for microscopy assistance and J. Gao (Shandong University) for providing the *Atoh1-Cre* and *Brg1^{fllox/fllox}* mice. Specifically, we thank Professor Bartles, J. R. (Northwestern University, USA) and Lili Zheng (Northwestern University, USA) for providing the purified pan-espin antibody and for productive discussion. This work was supported by the National Key R&D Program of China (2017YFA0103900), the Strategic Priority Research Program of the Chinese Academy of Science (XDA16010303), the National Natural Science Foundation of China (81622013, 81970882, 81470692, 81570919 and 31500852), Boehringer Ingelheim Pharma GmbH, the Natural Science Foundation of Jiangsu Province (BE2019711), and K.C. Wong Education Foundation.

Disclosure of conflict of interest

None.

Address correspondence to: Dr. Renjie Chai, Key Laboratory for Developmental Genes and Human

Disease, Ministry of Education, Institute of Life Sciences, Southeast University, Nanjing 210096, China. E-mail: renjiec@seu.edu.cn; Dr. Zengxin Qi, Department of Neurosurgery, Huashan Hospital, Fudan University, Shanghai 200040, China. E-mail: qizengxin123@163.com; Dr. Yunfeng Wang, ENT institute and Otorhinolaryngology Department of Eye & ENT Hospital, Fudan University, Shanghai 200031, China. E-mail: yunfengwang@fudan.edu.cn

References

- [1] Ashmore J. Cochlear outer hair cell motility. *Physiol Rev* 2008; 88: 173-210.
- [2] Ashmore JF. A fast motile response in guinea-pig outer hair cells: the cellular basis of the cochlear amplifier. *J Physiol* 1987; 388: 323-347.
- [3] Roberts WM, Howard J and Hudspeth AJ. Hair cells: transduction, tuning, and transmission in the inner ear. *Annu Rev Cell Biol* 1988; 4: 63-92.
- [4] Flock A and Cheung HC. Actin filaments in sensory hairs of inner ear receptor cells. *J Cell Biol* 1977; 75: 339-343.
- [5] Tilney LG, Derosier DJ and Mulroy MJ. The organization of actin filaments in the stereocilia of cochlear hair cells. *J Cell Biol* 1980; 86: 244-259.
- [6] Slepecky N and Chamberlain SC. Immunoelectron microscopic and immunofluorescent localization of cytoskeletal and muscle-like contractile proteins in inner ear sensory hair cells. *Hear Res* 1985; 20: 245-260.
- [7] Bartles JR. Parallel actin bundles and their multiple actin-bundling proteins. *Curr Opin Cell Biol* 2000; 12: 72-78.
- [8] Sekerková G, Zheng L, Mugnaini E and Bartles JR. Differential expression of espin isoforms during epithelial morphogenesis, stereociliogenesis and postnatal maturation in the developing inner ear. *Dev Biol* 2006; 291: 83-95.
- [9] Li H, Liu H, Balt S, Mann S, Corrales CE and Heller S. Correlation of expression of the actin filament-bundling protein espin with stereociliary bundle formation in the developing inner ear. *J Comp Neurol* 2004; 468: 125-134.
- [10] Sekerkova G, Richter CP and Bartles JR. Roles of the espin actin-bundling proteins in the morphogenesis and stabilization of hair cell stereocilia revealed in CBA/CaJ congenic jerker mice. *PLoS Genet* 2011; 7: e1002032.
- [11] Sekerkova G, Zheng L, Loomis PA, Changyaleket B, Whitton DS, Mugnaini E and Bartles JR. Espins are multifunctional actin cytoskeletal regulatory proteins in the microvilli of chemosensory and mechanosensory cells. *J Neurosci* 2004; 24: 5445-5456.

Espin distribution in stereocilia

- [12] Bartles JR, Wierda A and Zheng L. Identification and characterization of espin, an actin-binding protein localized to the F-actin-rich junctional plaques of Sertoli cell ectoplasmic specializations. *J Cell Sci* 1996; 109: 1229.
- [13] Salles FT, Merritt RC Jr, Manor U, Dougherty GW, Sousa AD, Moore JE, Yengo CM, Dosé AC and Kachar B. Myosin IIIa boosts elongation of stereocilia by transporting espin 1 to the plus ends of actin filaments. *Nat Cell Biol* 2009; 11: 443-50.
- [14] Roth B and Bruns V. Postnatal development of the rat organ of corti. II. hair cell receptors and their supporting elements. *Anat Embryol (Berl)* 1992; 185: 571-581.
- [15] Roth B and Bruns V. Postnatal development of the rat organ of corti. I. general morphology, basilar membrane, tectorial membrane and border cells. *Anat Embryol (Berl)* 1992; 185: 559-569.
- [16] Huang B, Babcock H and Zhuang X. Breaking the diffraction barrier: super-resolution imaging of cells. *Cell* 2010; 143: 1047-1058.
- [17] Harke B, Keller J, Ullal CK, Westphal V, Schonle A and Hell SW. Resolution scaling in STED microscopy. *Opt Express* 2008; 16: 4154-4162.
- [18] Westphal V, Rizzoli SO, Lauterbach MA, Kamin D, Jahn R and Hell SW. Video-rate far-field optical nanoscopy dissects synaptic vesicle movement. *Science* 2008; 320: 246-249.
- [19] Sidenstein SC, D'Este E, Bohm MJ, Danzl JG, Belov VN and Hell SW. Multicolour multilevel STED nanoscopy of actin/spectrin organization at synapses. *Sci Rep* 2016; 6: 26725.
- [20] Winter FR, Loidolt M, Westphal V, Butkevich AN, Gregor C, Sahl SJ and Hell SW. Multicolour nanoscopy of fixed and living cells with a single STED beam and hyperspectral detection. *Sci Rep* 2017; 7: 46492.
- [21] Gottfert F, Wurm CA, Mueller V, Berning S, Cordes VC, Honigsmann A and Hell SW. Coaligned dual-channel STED nanoscopy and molecular diffusion analysis at 20 nm resolution. *Biophys J* 2013; 105: L01-03.
- [22] Kelu JJ, Webb SE, Parrington J, Galione A and Miller AL. Ca(2+) release via two-pore channel type 2 (TPC2) is required for slow muscle cell myofibrillogenesis and myotomal patterning in intact zebrafish embryos. *Dev Biol* 2017; 425: 109-129.
- [23] Ruan H, Yu J, Yuan J, Li N and Fang X. Nanoscale distribution of transforming growth factor receptor on post-golgi vesicle revealed by super-resolution microscopy. *Chem Asian J* 2016; 11: 3359-3364.
- [24] Shang L, Gao P, Wang H, Popescu R, Gerthsen D and Nienhaus GU. Protein-based fluorescent nanoparticles for super-resolution STED imaging of live cells. *Chem Sci* 2017; 8: 2396-2400.
- [25] Barabas FM, Masullo LA, Bordenave MD, A Giusti S, Unsain N, Refojo D, Cáceres A and Stefani FD. Automated quantification of protein periodic nanostructures in fluorescence nanoscopy images: abundance and regularity of neuronal spectrin membrane-associated skeleton. *Sci Rep* 2017; 7: 16029.
- [26] Zhao B, Wu ZZ and Muller U. Murine Fam65b forms ring-like structures at the base of stereocilia critical for mechanosensory hair cell function. *Elife* 2016; 5: e14222.
- [27] Fong CS, Kim M, Yang TT, Liao JC and Tsou MF. SAS-6 assembly templated by the lumen of cartwheel-less centrioles precedes centriole duplication. *Dev Cell* 2014; 30: 238-245.
- [28] Ishigaki M, Iketani M, Sugaya M, Takahashi M, Tanaka M, Hattori S and Ohsawa I. STED super-resolution imaging of mitochondria labeled with TMRM in living cells. *Mitochondrion* 2016; 28: 79-87.
- [29] Bottanelli F, Kromann EB, Allgeyer ES, Erdmann RS, Wood Baguley S, Sirinakis G, Schepartz A, Baddeley D, Toomre DK, Rothman JE and Bewersdorf J. Two-colour live-cell nanoscale imaging of intracellular targets. *Nat Commun* 2016; 7: 10778.
- [30] Thompson AD, Omar MH, Rivera-Molina F, Xi Z, Koleske AJ, Toomre DK and Schepartz A. Long-term live-cell STED nanoscopy of primary and cultured cells with the plasma membrane HIDE probe Dil-SiR. *Angew Chem Int Ed Engl* 2017; 56: 10408-10412.
- [31] Zhao WD, Hamid E, Shin W, Wen PJ, Krystofiak ES, Villarreal SA, Chiang HC, Kachar B and Wu LG. Hemi-fused structure mediates and controls fusion and fission in live cells. *Nature* 2016; 534: 548-552.
- [32] Zhang WI, Rohse H, Rizzoli SO and Opazo F. Fluorescent in situ hybridization of synaptic proteins imaged with super-resolution STED microscopy. *Microsc Res Tech* 2014; 77: 517-527.
- [33] Daemen S, van Zandvoort MA, Parekh SH and Hesselink MK. Microscopy tools for the investigation of intracellular lipid storage and dynamics. *Mol Metab* 2016; 5: 153-163.
- [34] Xu K, Zhong G and Zhuang X. Actin, spectrin, and associated proteins form a periodic cytoskeletal structure in axons. *Science* 2013; 339: 452-456.
- [35] D'Este E, Kamin D, Gottfert F, El-Hady A and Hell SW. STED nanoscopy reveals the ubiquity of subcortical cytoskeleton periodicity in living neurons. *Cell Rep* 2015; 10: 1246-1251.
- [36] Lukinavicius G, Reymond L, D'Este E, Masharina A, Gottfert F, Ta H, Guther A, Fournier M, Rizzo S, Waldmann H, Blaukopf C, Sommer C, Gerlich DW, Arndt HD, Hell SW and Johnsson K. Fluorogenic probes for live-cell imaging of

Espin distribution in stereocilia

- the cytoskeleton. *Nat Methods* 2014; 11: 731-733.
- [37] Qi J, Liu Y, Chu C, Chen X, Zhu W, Shu Y, He S, Chai R and Zhong G. A cytoskeleton structure revealed by super-resolution fluorescence imaging in inner ear hair cells. *Cell Discov* 2019; 5: 12.
- [38] Liu Y, Qi J, Chen X, Tang M, Chu C, Zhu W, Li H, Tian C, Yang G, Zhong C, Zhang Y, Ni G, He S, Chai R and Zhong G. Critical role of spectrin in hearing development and deafness. *Sci Adv* 2019; 5: eaav7803.
- [39] Sekerková G, Zheng L, Mugnaini E and Bartles JR. Espin actin-cytoskeletal proteins are in rat type I spiral ganglion neurons and include splice-isoforms with a functional nuclear localization signal. *J Comp Neurol* 2008; 509: 661-676.
- [40] Loomis PA, Zheng L, Sekerková G, Changyaleket B, Mugnaini E and Bartles JR. Espin cross-links cause the elongation of microvillus-type parallel actin bundles in vivo. *J Cell Biol* 2003; 163: 1045.
- [41] Wang L, Zou J, Shen Z, Song E and Yang J. Whirlin interacts with espin and modulates its actin-regulatory function: an insight into the mechanism of usher syndrome type II. *Hum Mol Genet* 2012; 21: 692-710.
- [42] Jin Y, Ren N, Li S, Fu X, Sun X, Men Y, Xu Z, Zhang J, Xie Y, Xia M and Gao J. Deletion of *Brg1* causes abnormal hair cell planer polarity, hair cell anchorage, and scar formation in mouse cochlea. *Sci Rep* 2016; 6: 27124.
- [43] Merritt Raymond C, Manor U, Salles Felipe T, Grati MH, Dose Andrea C, Unrath William C, Quintero Omar A, Yengo Christopher M and Kachar B. Myosin IIIB uses an actin-binding motif in its espin-1 cargo to reach the tips of actin protrusions. *Curr Biol* 2011; 22: 320-325.
- [44] Pataky F, Pironkova R and Hudspeth AJ. Radixin is a constituent of stereocilia in hair cells. *P Natl Acad Sci U S A* 2004; 101: 2601-2606.
- [45] Ebrahim S, Avenarius MR, Grati M, Krey JF, Windsor AM, Sousa AD, Ballesteros A, Cui RJ, Millis BA, Salles FT, Baird MA, Davidson MW, Jones SM, Choi D, Dong LJ, Raval MH, Yengo CM, Barr-Gillespie PG and Kachar B. Stereocilia-staircase spacing is influenced by myosin III motors and their cargos espin-1 and espin-like. *Nat Commun* 2016; 7: 10833.